Journal of Nuclear Materials 464 (2015) 155–159

Contents lists available at ScienceDirect

Journal of Nuclear Materials

journal homepage: www.elsevier.com/locate/jnucmat

Creep strength and microstructure of F82H steels near tempering temperature

K. Shinozuka [a,*], H. Esaka [a], H. Sakasegawa [b], H. Tanigawa [b]

[a] National Defense Academy, Yokosuka, Kanagawa 239-8686, Japan
[b] Japan Atomic Energy Agency, Rokkasho, Aomori 039-3212, Japan

ARTICLE INFO

Article history:
Received 17 November 2013
Accepted 18 April 2015
Available online 24 April 2015

ABSTRACT

Creep rupture tests near the tempering temperature were performed, and the creep behavior at high temperatures and the structures of fracture specimens were investigated. Three kinds of F82H test specimens were used: IEA-heat, mod.3, and BA07. The time-to-rupture of the BA07 specimens was the longest under all the test conditions. This was because the minimum creep rates of BA07 were smallest, and a large quantity of fine precipitates of MX from the ESR treatment were considered to be effective in providing creep resistance. Although mod.3 specimens showed a high creep resistance under high stress, the time-to-rupture of mod.3 and IEA-heat were almost the same at low stress. This was because the fine tempered martensitic structure was weakened by being subjected to a high temperature for a long period. Therefore, it is considered that a large quantity of fine MX precipitates are effective for creep resistance near the tempering temperature.

1. Introduction

The reduced activation ferritic/martensitic (RAF/M) steel F82H is used for the blanket structures manufactured in Japan [1]. The strength of the welds in F82H is important because blanket manufacturing utilizes numerous welding processes [2,3]. However, only evaluating the strength of the welded F82H is insufficient. Microstructural develops and residual stress was induced into the steel upon welding, thereby reducing the creep strength. Therefore, Post-weld heat treatment (PWHT) is carried out to compensate for the strength reduction upon welding, and the creep tests were performed to attain the creep deformation rate in order to optimize the PWHT. In ferritic heat-resistant steels used for thermal power generation, PWHT is carried out at temperatures higher than 973 K. Thus, it is necessary to find the creep curves that include the high-temperature range for F82H. Serizawa et al. simulated the PWHT of F82H using the minimum creep rate at 823–923 K [4]. The minimum creep rate in the actual temperature of the PWHT will be required in order to perform more accurate calculation. The purpose of this research was to measure the exact minimum creep rate of F82H near PWHT temperature. It is necessary to examine whether the measured minimum creep rate is reliable from rupture time or a creep curve.

Furthermore, it is necessary to determine the microstructural changes in F82H to understand temper embrittlement that may occur during heat treatment at high temperatures. For these purposes, creep rupture tests were performed for F82H near the tempering temperature, and the creep behavior at high temperatures and the structures of fracture specimens were studied by the microscopes in this study.

2. Experimental

Three kinds of reduced activation martensitic steels (F82H) were used as specimens: IEA-heat [1], mod.3 and BA07 [5,6]. The standard chemical composition of F82H is Fe–0.1C–8Cr–2W–0.2V–0.02Ta (wt%). The chemical composition of each specimen is listed in Table 1. The amount of Ta in mod.3 was added up to 0.1 wt% in order to increase the amount of MX precipitates, and to refine the grains. The amount of Ta in BA07 was also increased to twice of that in IEA-heat, and an electro-slag remelting (ESR) treatment was carried out [5]. These steels were normalized at 1313 K for 30–40 min and then tempered at 1013–1023 K for 1 h.

The creep test specimens were machined parallel to the hot-rolled direction, and was 6 mm in diameter and had a gauge length of 30 mm. Creep rupture tests were performed at (i) 973 K in a stress range of 40–60 MPa and (ii) at 1023 K in a stress range of 30–50 MPa. The microstructures were observed using an optical microscope (OM; BX51M, Olympus Co.) and a transmission electron microscope (TEM; JEM-2100F, JEOL Ltd.). The specimens for

* Corresponding author. Tel.: +81 46 841 3810; fax: +81 46 844 5910.
E-mail address: kshinozu@nda.ac.jp (K. Shinozuka).

http://dx.doi.org/10.1016/j.jnucmat.2015.04.035
0022-3115/

Table 1
Chemical compositions of three kinds of F82H (wt%).

	C	Cr	W	V	Ta	N	Ti
IEA-heat	0.09	7.87	1.94	0.16	0.02	0.006	0.01
mod.3	0.10	7.92	1.87	0.21	0.10	0.009	<0.001
BA07	0.09	8.02	1.83	0.19	0.04	0.015	<0.003
							Fe: balance

OM observation were etched in a dilute solution of 1% picric acid and 5% hydrochloric acid in methanol in order to observe the tempered martensite structure after mirror finishing. The specimens for TEM observation were prepared by using a focused ion beam apparatus (FB-2100, Hitachi Ltd.) to ensure that they had about the same thickness (100 nm). The TEM (JED-2300T, JEOL Ltd.) was equipped with an energy dispersion X-ray spectrometer (EDS) to characterize the chemical compositions of microstructures.

3. Results and discussion

3.1. Creep tests

The time-to-rupture values for all the creep tests are listed in Table 2. BA07 had the longest time-to-rupture under all the conditions. Mod.3 had a longer time-to-rupture than IEA-heat, with the exception of the test under 30 MPa at 1023 K. Figs. 1 and 2 show the creep curves and the strain rates as a function of the strain in BA07, mod.3, and IEA-heat at 973 K, respectively. The curve of IEA-heat at 40 MPa only shows measurements for strains up to 8% because of an accidental failure of the ductilometer. Moreover, because the strain rate increased for strains greater than 20%, the ductilometer might have been unable to survey the elongation. However, the total elongation was found to be greater than 50% for all the crept specimens at 973 K and 1023 K. In all the creep tests, the creep curves showed transient creep until a strain of 1–2%, after which the creep accelerated. Corresponding to each stress, there was no significant difference in the minimum creep rates of the three kinds of steels. The creep rate of BA07 slowly increase after the moment achieving the minimum creep rate. In contrast, the creep rate of IEA-heat and mod.3 are much higher. If the region that shows a low creep rate is wide, the time-to-rupture should be lengthened. Therefore, it is considered that the slow acceleration near the minimum creep rate of the curves for BA07 contributed to the long time-to-rupture.

Figs. 3 and 4 show the creep curves and strain rate as functions of the strain in BA07, mod.3, and IEA-heat at 1023 K, respectively. The minimum creep rates were found at strains of 2–4% in all the creep tests, and the strain that showed the minimum creep rate became large in accordance with an increase in the strain rate, as shown in Fig. 4. Although there was no significant difference in the minimum creep rates of the three kinds of specimens at 973 K, the minimum creep rates of BA07 were lower than the rates of IEA-heat and mod.3 at 1023 K. A minimum creep rate is determined by the balance between the work hardening, dynamic recovery, and thermal recovery. Although the work hardening and dynamic recovery are mainly influenced by the strain, the thermal recovery is influenced by the elapsed creep time. If the strain rate increased, the thermal recovery was delayed relative to the work hardening and dynamic recovery, because the elapsed creep time was short. Therefore, the strain that indicated the minimum creep rate was considered to increase in accordance with an

Table 2
Time-to-rupture in creep tests of three kinds of F82H (h).

Temperature (K)	Stress (MPa)	BA07	mod.3	IEA-heat
973	60	111.7	85.0	78.9
	50	345.4	269.3	207.0
	40	1268.3	868.6	801.5
1023	50	10.0	9.8	7.8
	40	44.2	36.0	27.2
	30	178.0	92.4	100.0

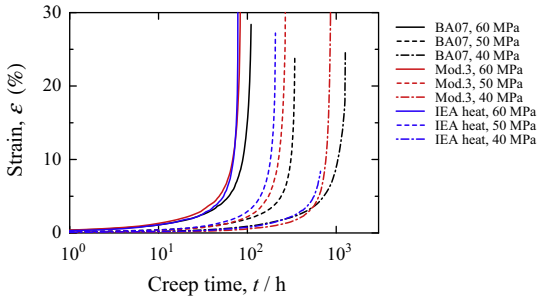

Fig. 1. Creep curves of BA07, mod.3, and IEA-heat at 973 K in stress range of 40–60 MPa.

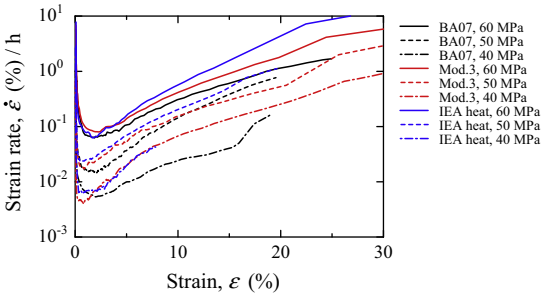

Fig. 2. Strain rates of BA07, mod.3, and IEA-heat at 973 K as function of strain.

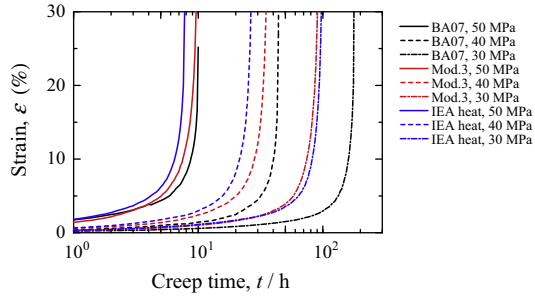

Fig. 3. Creep curves of BA07, mod.3, and IEA-heat at 1023 K in stress range of 30–50 MPa.

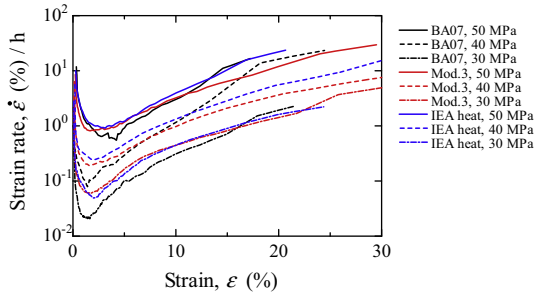

Fig. 4. Strain rates of BA07, mod.3, and IEA-heat at 1023 K as function of strain.

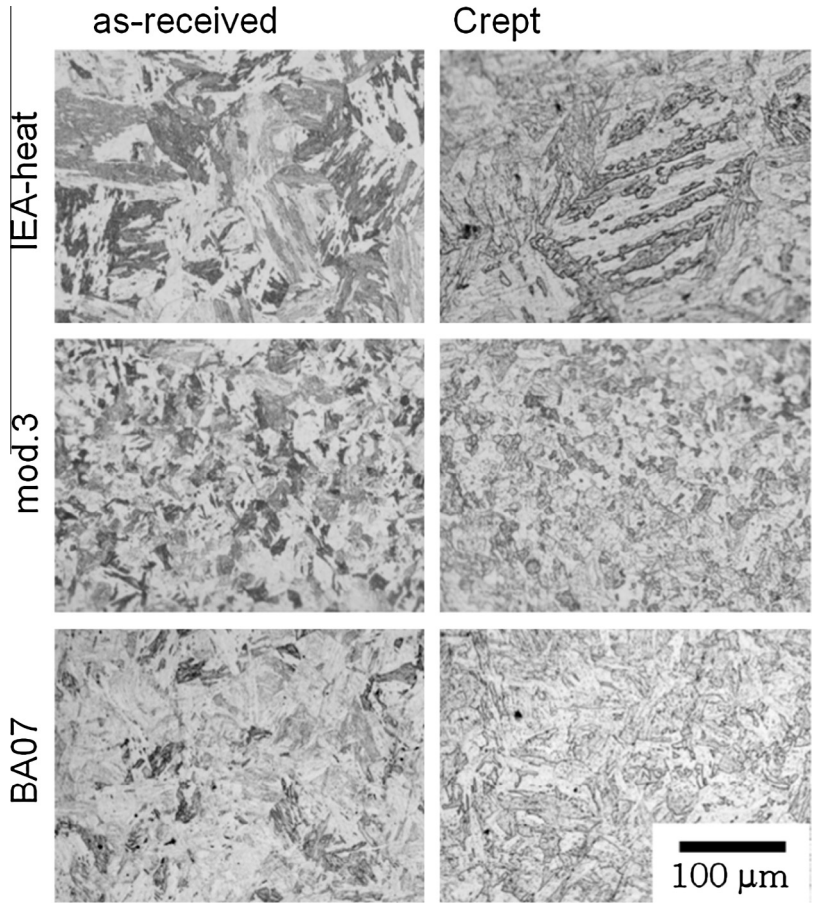

Fig. 5. Optical micrographs of as-received specimens and grip part of ruptured specimens at 1023 K and 40 MPa of BA07, mod.3, and IEA-heat.

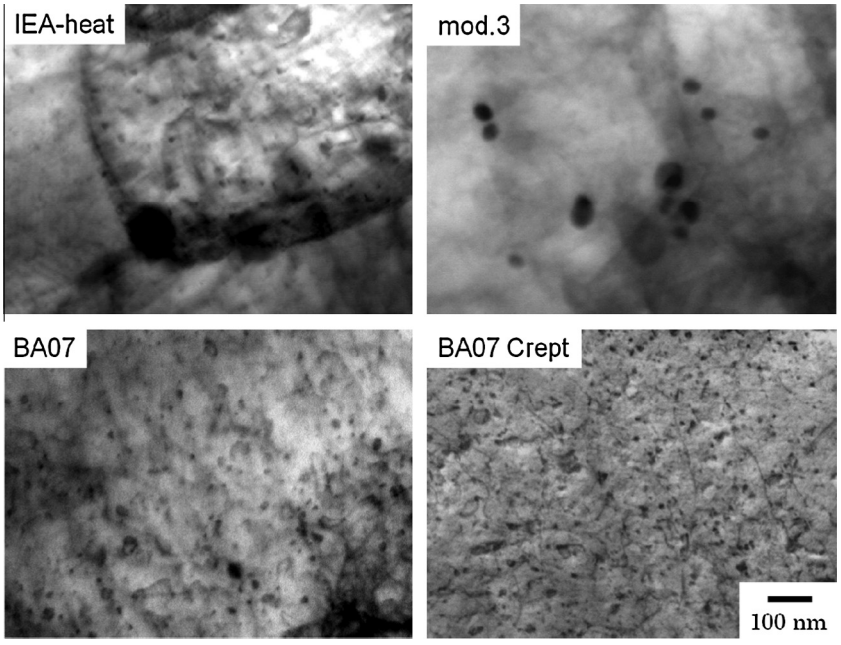

Fig. 6. Transmission electron micrographs of as-received specimen of BA07, mod.3, and IEA-heat and gauge part of ruptured specimen at 1023 K and 40 MPa of BA07.

increase in the strain rate, as shown in Fig. 4. Because dispersed particles are effective at retarding the thermal and dynamic recovery, the minimum creep rate of BA07 was smaller than the others at 1023 K. Although a similar phenomenon was seen at 973 K, there was no obvious difference in the minimum creep rate of each specimen. However, the creep curves of BA07 indicated a wider

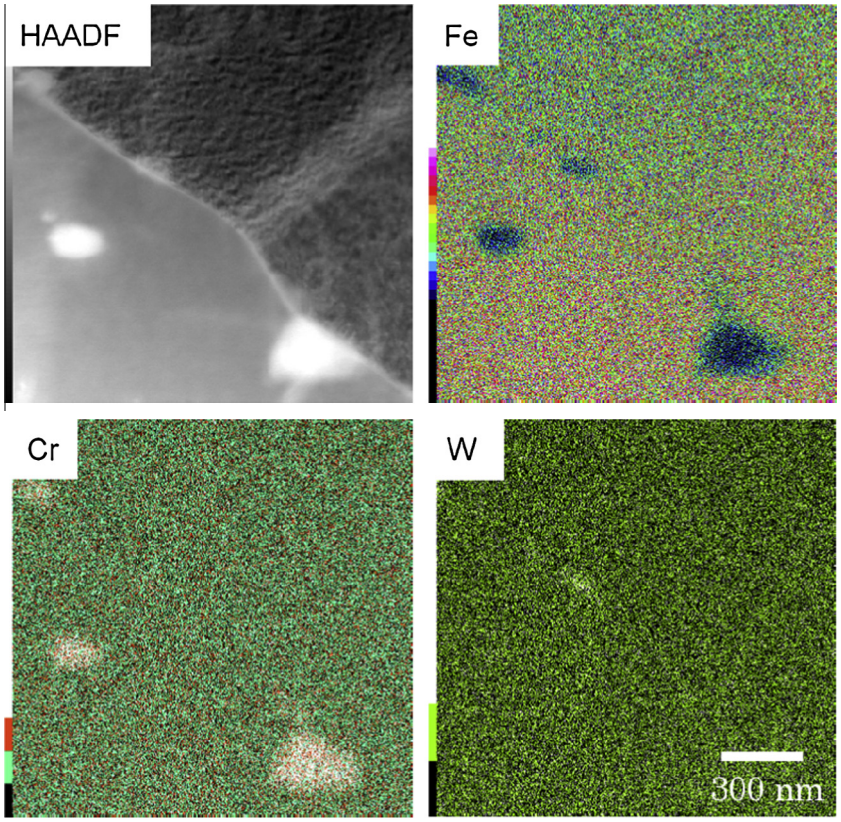

Fig. 7. Transmission electron micrograph and EDS analysis results of gauge part of ruptured specimen of BA07 at 1023 K and 40 MPa.

region where the strain rate was low compared to those for IEA-heat and mod.3. When the strain rate is low, a remarkable decrease in the acceleration of the strain rate by distributed oxide particles arises in oxide dispersion strengthened (ODS) steels. For example, in an ODS steel that contains Y–Ti–O complex oxides, but with almost the same chemical composition as F82H, the creep curve at 973 K and 191 MPa scarcely indicated the acceleration of the strain rate [7]. This is because the dynamic recovery and thermal recovery scarcely occurred as a result of the low strain rate and thermal stability of the oxide particles, respectively. The dispersion strengthened by MX particles in BA07 are also considered to have contributed to the delay in the recovery.

3.2. Microstructure

The recovery behavior is largely affected by the microstructure of a specimen. Optical micrographs of the as-received specimens and the grip part of the ruptured specimens of BA07, mod.3, and IEA-heat at 1023 K and 40 MPa are shown in Fig. 5. All the as-received specimens show typical tempering martensitic structures. The size of the prior austenite grain of the as-received IEA-heat is about 150 μm, and the grain sizes of mod.3 and BA07 are about 15 μm. The collapse of the packet and the block structure is confirmed in all the ruptured specimens. Fig. 6 shows transmission electron micrographs of the as-received specimen of BA07, mod.3, and IEA-heat. The particles in the photographs are estimated to be MX (M = Ta, V and X = C, N) from the EDS analysis and other studies [8,9]. In mod.3, there were few MX particles and they were coarse in comparison with IEA-heat and BA07. Therefore, as the effect of Ta addition up to 0.1 wt% in mod.3, the crystal grain of tempering martensitic structure was refined, but the number of MX particles scarcely increased in comparison with IEA-heat. In BA07, there were many MX particles in comparison with IEA-heat and these were fine particles of almost the same size as IEA-heat. Therefore, the ESR treatment is effective in the precipitation of fine MX particles [5]. Mod.3 showed the same creep strength as BA07 at 1023 K and 50 MPa, however, the rupture time of mod.3 and IEA were almost the same at 30 MPa, as shown in Fig. 3. Although mod.3 had effective strengthening by the martensitic structure under high stress, the effect was weaken due to the collapse of martensitic structure at high temperature. Although the martensitic structure in IEA-heat collapses, its impact is not significant due to (1) the relative large austenite grain, and (2) the strengthening of small MX type precipitates. On the other hand, it is considered the degradation of the martensite strengthening is insignificant for BA07 because its precipitation hardening by MX particles is dominant.

Fig. 6 also shows the micrographs of the gauge part of a ruptured specimen at 1023 K and 40 MPa of BA07. The size and number of the MX particles did not change obviously during creep tests. This agrees well with the study of the thermal stability of MX in F82H by Tamura et al. [9]. In addition, the creep mechanism in this study is considered to be the dislocation creep because the TEM images of BA07 show dislocation networks in the precipitate concentrated areas. The HAADF micrograph and EDS analysis results for the ruptured specimen are shown in Fig. 7. The EDS analysis confirmed that the particles were $M_{23}C_6$. Because the mean particle diameter of $M_{23}C_6$ in the as-received specimen was approximately 70 nm [10], it became coarser and approximately doubled in size. In addition, a particle composed of W existed in the grain boundary as shown in Fig. 7. It is known that these phenomena which decreased solid solute atoms are the cause of the decrease in creep resistance and the tempering embrittlement. On the other hand, due to the high thermal stability of MX precipitates, dispersion strengthening by MX in RAF/M is considered desirable to prevent tempering embrittlement.

4. Conclusions

The creep behavior near the tempering temperature of three kinds of RAF/M steel (F82H) was investigated, and the following conclusions were obtained.

1. BA07 shows the longest time-to-rupture at both 973 K and 1023 K. The minimum creep rate of BA07 was lower than those of mod.3 and IEA, especially at 1023 K.
2. Fine precipitates of MX were effective in providing creep resistance, and these particles did not coarsen when subjected to high temperatures for a long period. It is considered that there were many MX particles in BA07 from the ESR treatment.
3. Mod.3 showed a high creep resistance at high stress, and the time-to-rupture values of mod.3 and IEA were almost the same under low stress. This was because the finely tempered martensitic structure was weakened by being subjected to a high temperature for a long period of time.

References

[1] K. Shiba, M. Enoeda, S. Jitsukawa, J. Nucl. Mater. 329–333 (2004) 243–247.
[2] H. Tanigawa, T. Hirose, K. Shiba, R. Kasada, E. Wakai, H. Serizawa, Y. Kawahito, S. Jitsukawa, A. Kimura, Y. Kohno, A. Kohyama, S. Katayama, H. Mori, K. Nishimoto, R.L. Klueh, M.A. Sokolov, R.E. Stoller, S.J. Zinkle, Fusion Eng. Des. 83 (2008) 1471–1476.
[3] M. Rieth, J. Rey, J. Nucl. Mater. 386–366 (2009) 471–474.
[4] H. Serizawa, S. Nakamura, H. Tanigawa, H. Ogiwara, H. Murakawa, J. Nucl. Mater. 442 (2013) S535–S540.
[5] H. Sakasegawa, H. Tanigawa, S. Kano, M. Enomoto, Fusion Eng. Des. 86 (2011) 2541–2544.
[6] H. Tanigawa, K. Shiba, H. Sakasegawa, T. Hirose, S. Jitsukawa, Fusion Eng. Des. 86 (2011) 2549–2552.
[7] K. Shinozuka, M. Tamura, H. Esaka, K. Shiba, K. Nakamura, J. Nucl. Mater. 384 (2009) 1–5.
[8] H. Sakasegawa, H. Tanigawa, S. Kano, N. Enomoto, Fusion Eng. Des. 86 (2011) 2541–2544.
[9] M. Tamura, H. Kusuyama, K. Shinozuka, H. Esaka, J. Nucl. Mater. 367–370 (2007) 137–141.
[10] K. Fukumoto, T. Sakaguchi, K. Inoue, T. Itoh, H. Sakasegawa, H. Tanigawa, J. Nucl. Mater. 442 (2013) 528–532.